

Conserved Atomic Bonding Sequences and Strain Organization of Graphene Grain Boundaries

Haider I. Rasool,^{†,‡,○} Colin Ophus,^{§,○} Ziang Zhang,^{||,⊥,♯} Michael F. Crommie,^{†,‡,▽} Boris I. Yakobson,^{||,⊥,♯} and Alex Zettl*,^{†,‡,▽}

[†]Department of Physics and Center of Integrated Nanomechanical Systems (COINS), University of California at Berkeley, Berkeley, California 94720, United States

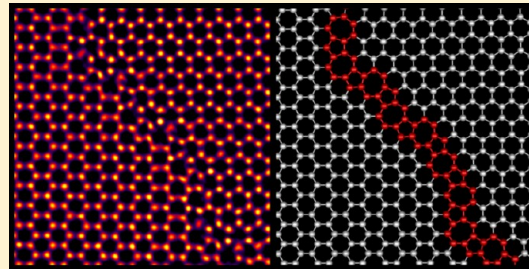
[‡]Materials Science Division and [§]National Center for Electron Microscopy (NCEM), Molecular Foundry, Lawrence Berkeley National Laboratory (LBNL), Berkeley, California 94720, United States

^{||}Department of Materials Science and NanoEngineering, [⊥]Department of Chemistry, and [#]Smalley Institute for Nanoscale Science and Technology, Rice University, Houston, Texas 77005, United States

[▽]Kavli Energy NanoSciences Institute at the University of California, Berkeley, California 94720, United States

S Supporting Information

ABSTRACT: The bulk properties of polycrystalline materials are directly influenced by the atomic structure at the grain boundaries that join neighboring crystallites. In this work, we show that graphene grain boundaries are comprised of structural building blocks of conserved atomic bonding sequences using aberration corrected high-resolution transmission electron microscopy. These sequences appear as stretches of identically arranged periodic or aperiodic regions of dislocations. Atomic scale strain and lattice rotation of these interfaces is derived by mapping the exact positions of every carbon atom at the boundary with ultrahigh precision. Strain fields are organized into local tensile and compressive dipoles in both periodic and aperiodic dislocation regions. Using molecular dynamics tension simulations, we find that experimental grain boundary structures maintain strengths that are comparable to idealized periodic boundaries despite the presence of local aperiodic dislocation sequences.



KEYWORDS: Graphene, grain boundary, aberration corrected TEM, strain, molecular dynamics, fracture

In polycrystalline materials, grain boundaries are the interfaces between two adjoining single crystals. For two-dimensional (2D) materials,^{1–3} grain boundaries are one-dimensional (1D) interfaces with distinct bonding configurations when compared to bulk crystallites.^{4–17} In polycrystalline graphene, our current theoretical understanding of the mechanical and electronic transport properties of grain boundaries is limited to idealized cases where these interfaces are modeled as periodic arrays of dislocations arranged in a straight line between neighboring crystallites.^{4–8} For polycrystalline graphene grown in the laboratory, synthesis has been shown to produce interfaces with meandering structures comprised of pentagons and heptagons (5–7 dislocations) that depart markedly from the idealized cases.^{14–17} The initial TEM characterizations of graphene grain boundaries imaged short stretches of atomically clean regions, making it difficult to observe long-range structural order.^{14,15} Although recent experiments have been performed to study the mechanical strength^{17–19} and electronic behavior of graphene grain boundaries,^{20–22} there are limited reports on the direct observations of its atomic structure.^{14,15,17} To understand the macroscopic properties of polycrystalline graphene films and implement the material in commercial scale processes, it is necessary to obtain high quality atomic structure information on

grown graphene and bridge the gap between experimental observations and theoretical predictions.

In this work, we present large area graphene grain boundary structures and atomic scale strain field maps derived from aberration corrected high-resolution transmission electron microscope (AC-HRTEM) images. Boundary interfaces are found to be comprised of local structural building blocks of conserved atomic bonding sequences of pentagons and heptagons. The exact atomic positions of carbon atoms in the lattice are measured with an ultrahigh precision of 4 pm. These positions are used to determine the quantitative magnitude and spatial distribution of strain fields along the boundaries. Surprisingly, strain fields are ordered into strain dipoles at the boundaries where adjacent areas of tensile strain balance areas of compressive strain,¹¹ despite aperiodic arrangements of 5–7 dislocations. Additionally, strain fields are highly localized near the boundary and decay rapidly into the adjacent single crystal lattices. Lastly, we perform molecular dynamics (MD) tension simulations that reveal that experimental boundary structures

Received: September 9, 2014

Revised: October 22, 2014

Published: November 6, 2014



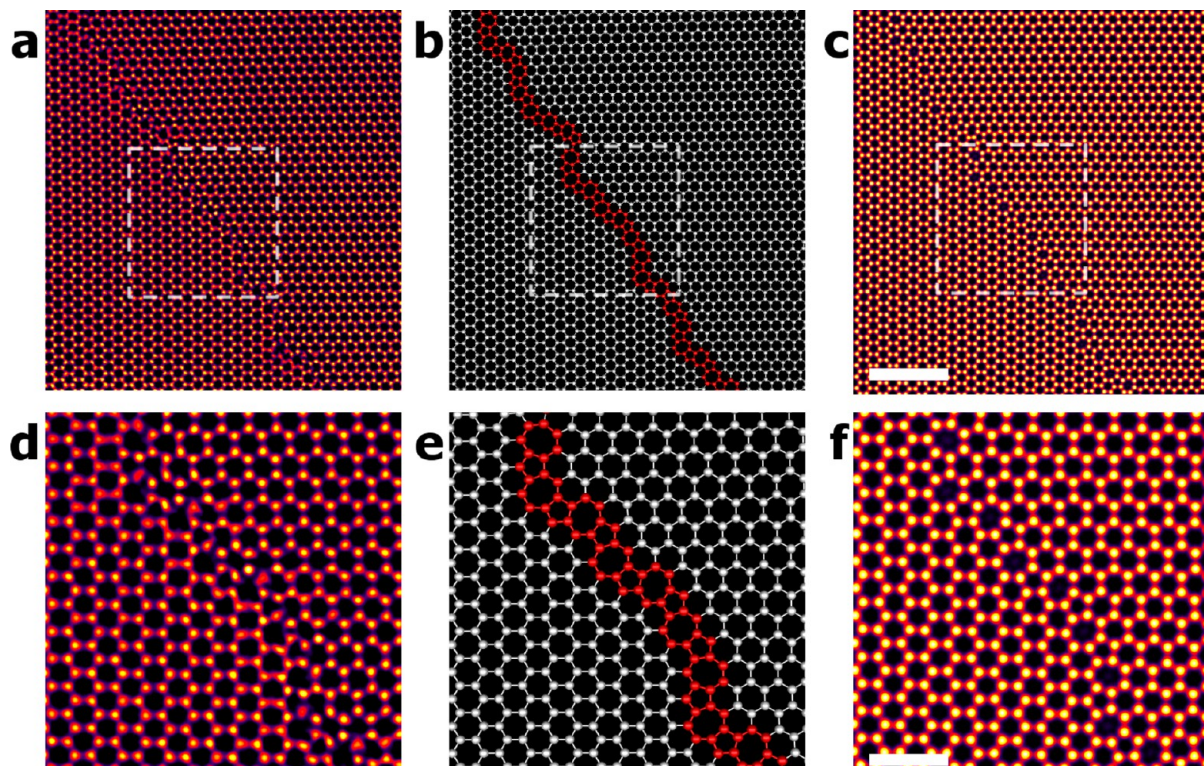


Figure 1. Atomic structure of a graphene grain boundary. (a) Large area exit wave intensity of a graphene grain boundary. (b) Atomic model and (c) simulated HRTEM image of (a). Carbon atoms and bonds at the boundary interface are colored red for clarity. (d–f), Images from the white boxed regions from panels a–c, respectively. Each zoomed region depicts the same area of the micrograph. Scale bars for (a–c) are 1.5 nm and for (d–f) are 0.75 nm.

with mixed regions of periodic and aperiodic sequences of dislocation have comparable fracture strength to theoretical idealized periodic structures.

Polycrystalline graphene is first grown by low-pressure chemical vapor deposition (CVD) on a copper catalyst²³ and subsequently transferred to a TEM grid. Samples are prepared using a polymer free direct transfer method, which produces large areas of atomically clean graphene. The fabrication is similar to previously reported methods,²⁴ but ammonium persulfate is used as a gentle chemical etchant to remove the copper growth catalyst. This etchant has recently been shown to improve the quality of transfer and minimize processing debris.¹⁹ Full details of the graphene growth and sample preparation is provided in the Supporting Information. Figure 1a shows the intensity of the electron exit wave function obtained from a focal series of a long length of an atomically clean graphene grain boundary. The grain boundary regions presented in the current work remain stable under the electron beam during acquisition of multiple focal series data sets with no observed beam effects. From the large area image, we derive an atomic model of the sheet (Figure 1b) and simulate an HRTEM (Figure 1c) image of the structure for comparison. Upon close inspection, it is clear that the position of every carbon atom can be unambiguously identified (Figure 1d) along the boundary. The edge atoms of the two different sheets comprising the grain boundary are stitched together via pentagons and heptagons along the boundary line and are highlighted in red in the atomic model (Figure 1b,e).

When two graphene grains meet during the growth process, edges of opposing sheets fuse together and form a 1D interface of bridging bonds to form a continuous 2D sheet. At the boundary, the nearby lattice atoms distort to accommodate local lattice mismatch between the two crystallites. The precise location of

the carbon atoms are measured directly from TEM images and compared to expected positions of an ideal graphene lattice to create 2D displacement maps. This real space analysis method is only possible when every atom can be clearly identified and has been used to study shear strain in single-walled carbon nanotubes and electric dipoles in ion columns of ferroelectric films.^{25,26} For images of isolated defect structures in a single crystal region of graphene, a Fourier space method known as gradient phase analysis (GPA) has been used to obtain strain fields from TEM micrographs.²⁷ In our real space analysis, the 2D displacement maps are constructed in the parallel (x -axis) and perpendicular (y -axis) directions along the boundary. A TEM image of a grain boundary, an atomic structural model, and displacement maps of a short stretch of a typical grain boundary are shown in Figure 2a–d. Atoms that are shifted to the right (up) appear red and atoms that are shifted left (down) appear blue in the displacement maps of Figure 2c,d. While displacement maps of the lattice indicate a measurable amount of distortion, it does not indicate regions of local lattice compression or tension.

To map local lattice strain and rotation, the displacement maps are numerically differentiated to provide gradient maps. For cases where local out-of-plane warping is minimal, as is the case in high-angle graphene grain boundaries, the 2D displacement gradient maps can be directly related to the strain of the material. The maps of the parallel (ϵ_{xx}), perpendicular (ϵ_{yy}), and shear (ϵ_{xy}) strain and local lattice rotation (θ) are presented in Figure 2e–h. A number of striking features appear immediately when looking at these maps. First, the strain is highly localized at the boundary, only propagating into the surrounding lattice by approximately 1 to 2 nm. Second, the magnitude of the maximum strain calculated in any of the strain fields is approximately 1 to 2%, which is minimal considering that graphene is predicted

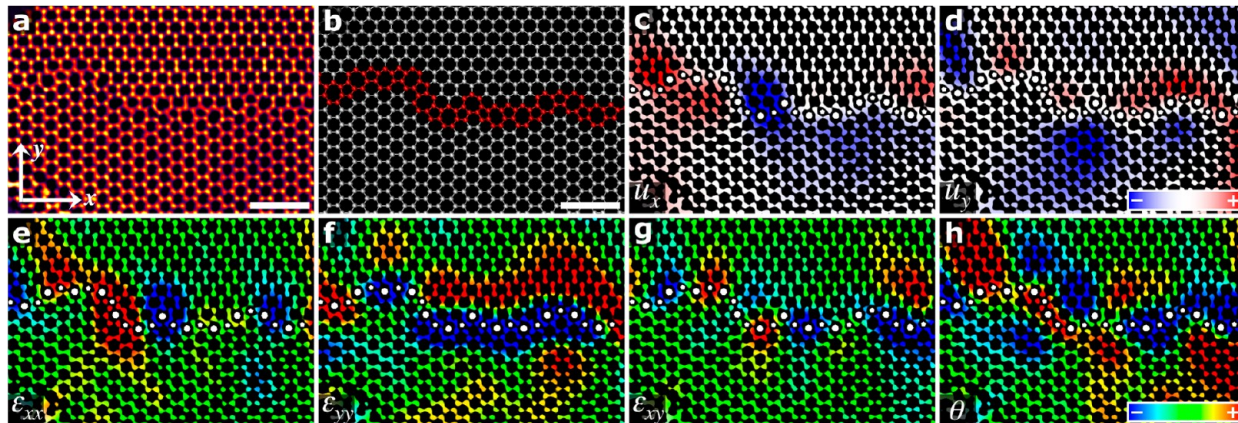


Figure 2. Strain organization at a graphene grain boundary. (a) Exit wave intensity of a graphene grain boundary. (b) Atomic model of (a). (c) Displacement map in the x -direction. (d) Displacement map in the y -direction. (e) Parallel strain, ϵ_{xx} . (f) Perpendicular strain, ϵ_{yy} . (g) Shear strain, ϵ_{xy} . (h) Local lattice rotation, θ . The color scale is $\pm 4\%$ for (c) and (d). The color scale is $\pm 1.25\%$ for (e–h). The color scale is $\pm 0.5^\circ$ for (h).

to experience tensile strains of approximately 20% before fracturing during uniaxial stretching.⁸

The most notable characteristic of the strain fields is that they are ordered into tension-compression dipoles with similar magnitudes and spatial extent along the boundary. For the parallel (Figure 2e) and perpendicular (Figure 2f) directions, the strain dipoles are aligned with their respective directions. Strain dipoles at the boundary are the result of local site mismatch between the two grains. As the two sheets stitch together during the growth process, certain atoms will be nearly perfectly poised to bond with the neighboring lattice without any local distortion. Other regions will need to be locally displaced to optimize stitching between the two lattices. If only a few of these atoms are displaced during the bonding of the two crystals with the surrounding lattice remaining fixed, than it is expected that compression will occur on the side of the displacement. In the direction opposite the displacement, a region of tension is expected to develop.

When observing short stretches of these 1D interfaces, it appears as though the two crystals are erratically fused together with a random assortment of pentagon–heptagon pairs. This is what has been suggested from previous HRTEM observations of short stretches of graphene grain boundaries.^{14,15,17} However, imaging different large areas of atomically clean grain boundaries, we find that they are comprised of structural units of conserved atomic bonding sequences and stretches of repeat units with conserved strain fields. The length of grain boundary regions comprised entirely of repeat units is likely related to the edge morphology of growing islands, which depend on the details of the growth conditions.^{28–30} Recently, STM experiments have shown evidence for the existence of small stretches of ordered grain boundary structures, however, these high-resolution studies image the local electronic structure rather than the carbon lattice directly.^{31–33}

A conserved atomic bonding sequence found in two separate regions of a graphene grain boundary is shown in Figure 3. In the central region of the HRTEM images (Figure 3a,b), the identical dislocation structures (Figure 3c,d) create nearly identical localized distortions in the surrounding single crystal lattices. In each strain field map, the spatial extent and quantitative magnitude of the strain fields matches well, despite the existence of different flanking regions of dislocations along the boundary (Figure 3e–l). These structural units of conserved sequences are found throughout the length of graphene grain boundaries and

provide a means for understanding these 1D interfaces from a structural building block perspective.

While aperiodic building blocks can appear in grain boundary structures, we also observe regions of periodically ordered structures which are related to ideal theoretical structures. One experimental structure (GB1) we observe is shown in Figure 4a,b and is related to a $28^\circ(3,1)(3,1)$ symmetric tilt boundary. In GB1, two sets of dislocation sequences (white boundary atoms in Figure 4b) are arranged in a periodic 1D chain with a noticeable kink (purple boundary atoms in Figure 4b) present in the central region. In the periodic region of the structure, periodic strain and lattice rotations occur at the boundary with the same spatial frequency of the $(3,1)(3,1)$ unit cell. The parallel and shear strain show periodic compressive strain with a magnitude of approximately 1% and a spatial extent of half the $(3,1)(3,1)$ unit cell with neutral strain regions between. Interestingly, in the perpendicular map, the strain mixes to form a narrow continuous field localized at the boundary while the local lattice rotation shows periodic dipoles arranged along the periodic arrangement of dislocations. These observations are consistent with theoretical predictions on periodic grain boundary structures.^{8,11} Near the kinked region of the boundary, an increase in strain and lateral extent of the strain fields is observed, but the strain dipole organization persists. The tension–compression strain and local rotation dipole structures are preserved in the kinked region as can be seen in Figure 4.

Another grain boundary structure (GB2) is presented in Figure 5, which contains a conserved atomic sequence that is replicated (Figure 5b). The fundamental unit of the sequence is a variation of a possible $(7,0)(4,4)$ asymmetric boundary that joins the armchair edge of one grain with the zigzag edge of another. In the $(7,0)(4,4)$ region, the strain dipoles in the parallel and perpendicular directions are repeated where the structural sequence is identical. In the parallel direction, the strain dipole occurs at the heptagon that joins the two units. In the perpendicular direction, compression exists along the flat region of the sequence and is balanced by a region of tension in the upper lattice.

The remaining portion of GB2 has an aperiodic sequence of 5–7 dislocations. Short stretches of the structure are related to the $(7,0)(4,4)$ structure and its half unit through mirror reflections or different Stone–Wales rotations. Surprisingly, the negative shear strain and local lattice rotation in the aperiodic region balances in magnitude and lateral extent the positive shear

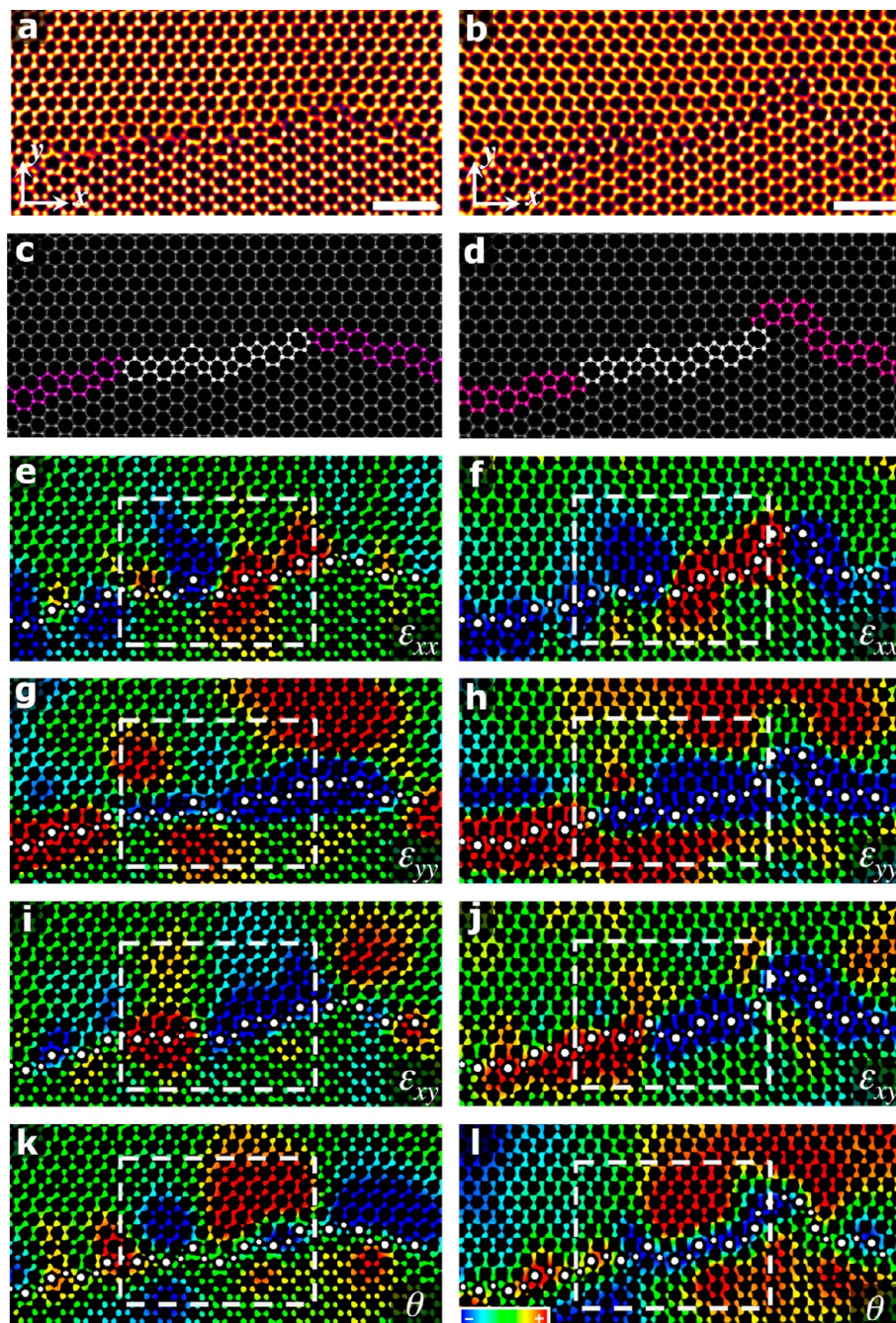


Figure 3. Conserved atomic bonding sequences of graphene grain boundaries. (a,b) Exit wave intensity of two different grain boundary regions. (c,d) Atomic models of (a,b). (e,f) Parallel strain, ϵ_{xx} . (g,h) Perpendicular strain, ϵ_{yy} . (i,j) Shear strain, ϵ_{xy} . (k,l) Local lattice rotation, θ . The color scale is $\pm 1.25\%$ for (e–j). The color scale is $\pm 0.5^\circ$ for (k,l).

strain and local lattice rotation observed in the ordered $(7,0)|(4,4)$ region of the boundary.

Because CVD graphene grown in the laboratory contains grain boundaries with a mixed arrangement of periodic and aperiodic dislocation sequences, it is important to understand how these structures affect its mechanical properties. Using atomic models from our experimental structures, we perform MD tension simulations to compare the failure strength of experimental grain boundaries with theoretical periodic structures. Figure 6 shows the results of four MD tension simulations. The first pair of simulations compares the GB1 structure from Figure 4 and the related theoretical $(3,1)|(3,1)$ symmetric periodic grain boundary. The second pair of simulations compares the GB2 structure

from Figure 5 and a theoretical boundary comprised of $(7,0)|(4,4)$ periodic units arranged linearly along the zigzag-armchair interface. To the best of the authors' knowledge, this is the first reporting of the tensile strength of this $(7,0)|(4,4)$ periodic structure.

The results of the comparative simulations reveal that graphene grain boundaries can tolerate local dislocation disorder without substantial degradation of the mechanical strength. The GB1 structure with the sharp kink in the center of the boundary fails at 92.5 GPa. The related theoretical $(3,1)|(3,1)$ symmetric periodic structure fails at 97.1 GPa, which represents a 5% decrease in yield strength between the kinked and perfect structure. This can be attributed to the slight increase in perpendicularly

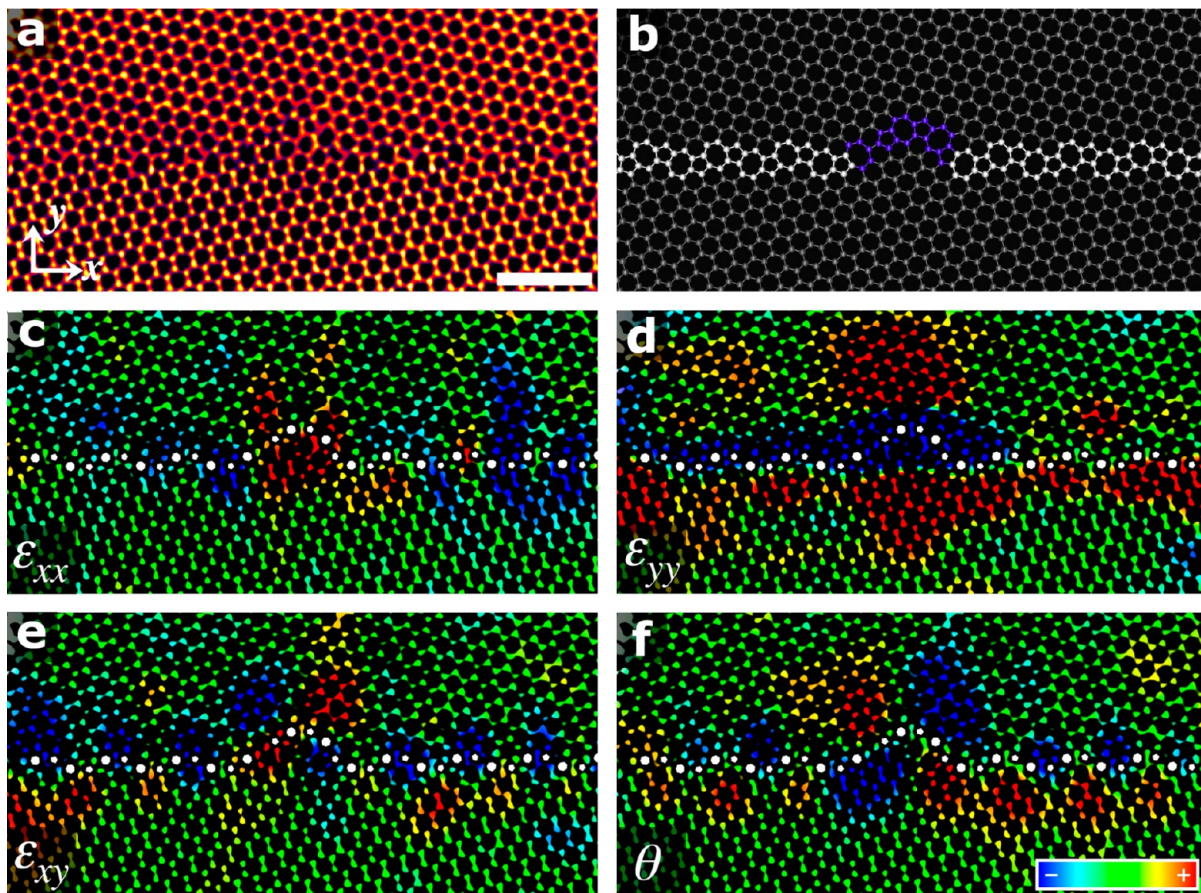


Figure 4. Symmetric experimental graphene grain boundary. (a) Exit wave intensity of a symmetric grain boundary region. (b) Atomic model of (a), highlighting the $(3,1)!(3,1)$ periodic conserved sequence. (c) Parallel strain, ϵ_{xx} . (d) Perpendicular strain, ϵ_{yy} . (e) Shear strain, ϵ_{xy} . (f) Local lattice rotation, θ . The scale bar for all images shown is given in (a) and is 1 nm. The color scale is $\pm 0.8\%$ for (c–e). The color scale is $\pm 0.5^\circ$ for (f).

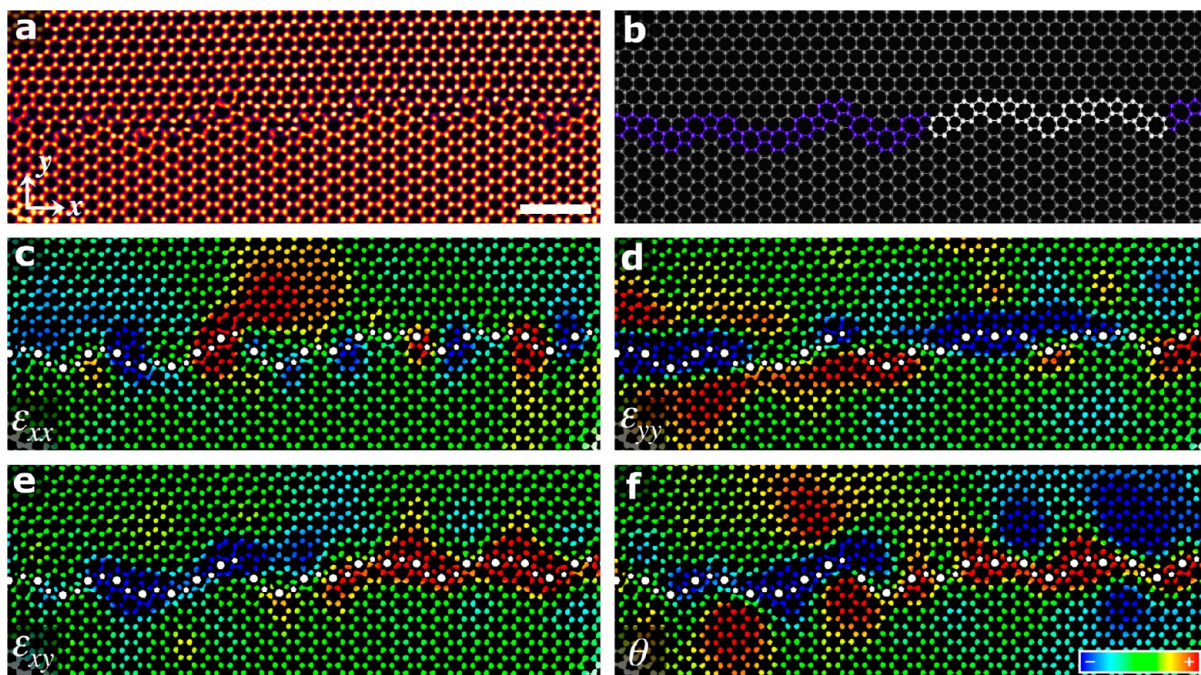


Figure 5. Asymmetric experimental graphene grain boundary. (a) Exit wave intensity of an asymmetric grain boundary region. (b) Atomic model of (a), highlighting the $(7,0)!(4,4)$ region of the boundary. (c) Parallel strain, ϵ_{xx} . (d) Perpendicular strain, ϵ_{yy} . (e) Shear strain, ϵ_{xy} . (f) Local lattice rotation, θ . The scale bar for all images shown is given in (a) and is 1 nm. The color scale is $\pm 1.0\%$ for (c–e). The color scale is $\pm 0.5^\circ$ for (f).

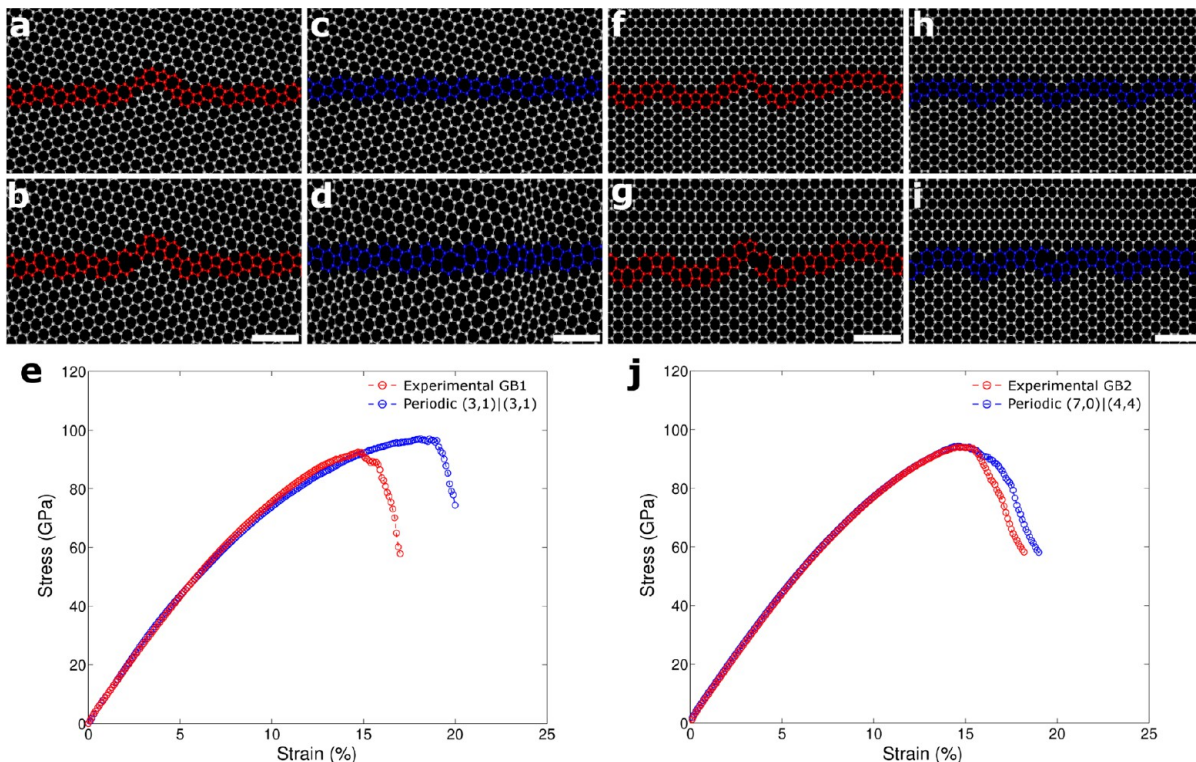


Figure 6. MD tension simulations of experimental and theoretical periodic boundaries. (a) Initial and (b) point of fracture structure of experimental GB1. (c) Initial and (d) point of fracture (3,1)|(3,1) symmetric periodic boundary. (e) Stress–strain curve for uniaxial tension simulation of GB1 and the (3,1)|(3,1) periodic boundary. (f) Initial and (g) point of fracture structure of experimental GB2. (h) Initial and (i) point of fracture (7,0)|(4,4) symmetric periodic boundary. (j) Stress–strain curve for uniaxial tension simulation of GB2 and the (7,0)|(4,4) periodic boundary. Scale bar for all atomic models are 1 nm.

strain in the kinked region of the boundary (Figure 3e). Surprisingly, GB2 has a failure strength that is nearly identical to the theoretical (7,0)|(4,4) structure. The theoretical structure fails at 94.3 GPa and the experimental structure fails at 94.0 GPa and can be understood by comparing the (7,0)|(4,4) replicated region of the experimental structure with the highly disordered sequence of 5–7 defects. In both regions of the boundary, they are under a constant minimal strain with no significant differences in strain magnitude despite the presence of dislocation disorder.

In summary, we use AC-HRTEM imaging to elucidate the atomic structure of long stretches of graphene grain boundaries. We find that these 1D interfaces contain a much greater degree of structural order than has been previously observed by HRTEM. The grain boundaries are found to be comprised of structural building blocks of conserved sequences of dislocations that give rise to similar perturbations to the surrounding single crystal lattice. The structural units can appear as local aperiodic or periodic sequences. For periodic dislocation sequences, we observe periodic strain dipoles in the lattice surrounding the grain boundary. Surprisingly, regions with kinks and aperiodic arranged 5–7 dislocations generate ordered strain dipoles with magnitudes that are comparable to ideal periodic structures. Lastly, MD tension simulations reveal that experimental structures with aperiodic sequences of dislocations maintain strengths of related theoretical ideal structures.

■ ASSOCIATED CONTENT

Supporting Information

The details of the CVD growth of graphene, TEM sample preparation, and strain analysis are included with supporting

figures for strain analysis and MD simulations. This material is available free of charge via the Internet at <http://pubs.acs.org>.

■ AUTHOR INFORMATION

Corresponding Author

*E-mail: azettl@berkeley.edu.

Author Contributions

○ H.I.R. and C.O. contributed equally to this work.

Notes

The authors declare no competing financial interest.

■ ACKNOWLEDGMENTS

H.I.R. and A.Z. acknowledge support in part by the Director, Office of Basic Energy Sciences, Materials Sciences and Engineering Division, of the U.S. Department of Energy under Contract DE-AC02-05CH11231, within the sp₂-bonded Materials Program, which provided for detailed TEM characterization; the National Science Foundation under grant DMR-1206512, which provided for Raman characterization; and the Office of Naval Research under grant N00014-12-1-1008 which supported graphene synthesis and transfer. C.O. acknowledges support by the National Center for Electron Microscopy (NCEM) of the Lawrence Berkeley National Laboratory (LBNL), under Contract DE-AC02-05CH11231. Z.Z. and B.I.Y. acknowledge support from the Office of Naval Research (MURI) and from the National Science Foundation CMMI (EAGER Grant 0951145).

■ REFERENCES

- (1) Novoselov, K. S.; et al. *Proc. Natl. Acad. Sci. U.S.A.* **2005**, *102*, 10451–10453.
- (2) Novoselov, K. S.; et al. *Nature* **2005**, *438*, 197.

- (3) Zhang, Y.; Tan, Y.-W.; Stormer, H. L.; Kim, P. *Nature* **2005**, *438*, 201.
- (4) Yazyev, O. V.; Louie, S. G. *Phys. Rev. B* **2010**, *81*, 195420.
- (5) Yazyev, O. V.; Louie, S. G. *Nat. Mater.* **2010**, *9*, 806.
- (6) Liu, Y.; Yakobson, B. I. *Nano Lett.* **2010**, *10*, 2178.
- (7) Grantab, R.; Shenoy, V. B.; Ruoff, R. S. *Science* **2010**, *330*, 946.
- (8) Wei, Y.; et al. *Nat. Mater.* **2012**, *11*, 759.
- (9) Najmaei, S.; et al. *Nat. Mater.* **2013**, *12*, 754–759.
- (10) van der Zande, A. M.; et al. *Nat. Mater.* **2013**, *12*, 554–561.
- (11) Yakobson, B. I.; Ding, F. *ACS Nano* **2013**, *5*, 253.
- (12) Liu, Y.; Zou, X.; Yakobson, B. I. *ACS Nano* **2012**, *6*, 7053–7058.
- (13) Gibb, A. L.; et al. *J. Am. Chem. Soc.* **2013**, *18*, 6758–6761.
- (14) Kim, K.; et al. *ACS Nano* **2011**, *5*, 2142.
- (15) Huang, P. Y.; et al. *Nature* **2011**, *469*, 389.
- (16) Coraux, J.; N'Diaye, A. T.; Busse, C.; Michely, T. *Nano Lett.* **2008**, *8*, 565.
- (17) Rasool, H. I.; Ophus, C.; Klug, W. S.; Zettl, A.; Gimzewski, J. K. *Nat. Commun.* **2013**, *4*, 2811.
- (18) Ruiz-Vargas, C. S.; et al. *Nano Lett.* **2011**, *11*, 2259.
- (19) Lee, G.-H.; et al. *Science* **2013**, *340*, 1073.
- (20) Yu, Q.; et al. *Nat. Mater.* **2011**, *10*, 443–449.
- (21) Tsen, A. W.; et al. *Science* **2012**, *336*, 1143.
- (22) Jauregui, L. A.; Cao, H.; Wu, W.; Yu, Q.; Chen, Y. P. *Solid State Commun.* **2011**, *151*, 1100.
- (23) Li, X.; et al. *Science* **2009**, *324*, 1312.
- (24) Regan, W.; et al. *Appl. Phys. Lett.* **2010**, *96*, 113102.
- (25) Jia, C. L.; et al. *Nat. Mater.* **2008**, *7*, 57–61.
- (26) Warner, J. H.; Young, N. P.; Kirkland, A. I.; Briggs, G. A. D. *Nat. Mater.* **2011**, *10*, 958–962.
- (27) Warner, J. H.; et al. *Science* **2012**, *337*, 209.
- (28) Nie, S.; Wofford, J. M.; Bartlet, N. C.; Dubon, O. D.; McCarty, K. F. *Phys. Rev. B* **2011**, *84*, 155425.
- (29) Vlassiouk, I.; et al. *ACS Nano* **2011**, *5*, 6096.
- (30) Hao, Y.; et al. *Science* **2013**, *342*, 720.
- (31) Lahiri, J.; Lin, Y.; Bozkurt, P.; Oleynik, I. I.; Batzill, M. *Nat. Nanotechnol.* **2010**, *5*, 326.
- (32) Ma, C.; et al. *Phys. Rev. Lett.* **2014**, *112*, 226802.
- (33) Yang, B.; Xu, H.; Lu, J.; Loh, K. P. *J. Am. Chem. Soc.* **2014**, *136* (34), 12041–12046.